ACS OMEGA

http://pubs.acs.org/journal/acsodf

Article

# Patterning GaSe by High-Powered Laser Beams

Dmitry Cheshev, Raul D. Rodriguez,* Aleksandar Matković, Alexey Ruban, Jin-Ju Chen, and Evgeniya Sheremet

Cite This: *ACS Omega* 2020, 5, 10183−10190

Read Online

ACCESS | Metrics & More | Article Recommendations

**ABSTRACT:** We report the high-powered laser modification of the chemical, physical, and structural properties of the two-dimensional (2D) van der Waals material GaSe. Our results show that contrary to expectations and previous reports, GaSe at the periphery of a high-power laser beam does not entirely decompose into Se and $Ga_2O_3$. In contrast, we find unexpectedly that the Raman signal from GaSe gets amplified around regions where it was not expected to exist. Atomic force microscopy (AFM), dielectric force microscopy (DFM), scanning electron microscopy (SEM), and energy-dispersive X-ray spectroscopy (EDX) results show that laser irradiation induces the formation of nanoparticles. Our analyses demonstrate that, except for a fraction of $Ga_2Se_3$, these nanoparticles still belong to the GaSe phase but possess different electrical and optical properties. These changes are evidenced in the increased Raman intensity attributed to the near-resonance conditions with the Raman excitation laser. The elemental analysis of nanoparticles shows that the relative selenium content increased to as much as 70% from a 50:50 value in stoichiometric GaSe. This elemental change is related to the formation of the $Ga_2Se_3$ phase identified by Raman spectroscopy at some locations near the edge. Further, we exploit the localized high-power laser processing of GaSe to induce the formation of Ag−GaSe nanostructures by exposure to a solution of $AgNO_3$. The selective reaction of $AgNO_3$ with laser-irradiated GaSe gives rise to composite nanostructures that display photocatalytic activity originally absent in the pristine 2D material. The photocatalytic activity was investigated by the transformation of 4-nitrobenzenethiol to its amino and dimer forms detected *in situ* by Raman spectroscopy. This work improves the understanding of light−matter interaction in layered systems, offering an approach to the formation of laser-induced composites with added functionality.

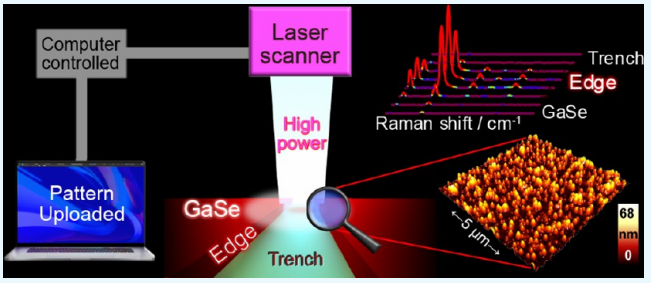




## INTRODUCTION

From graphene to other two-dimensional (2D) materials like metal dichalcogenides and graphene oxide,[1,2] research groups around the globe are continuing to create, investigate, and modify these materials as well as finding ways to apply them as photodetectors, transistors, and a range of sensors.[3−5] Although the pristine properties of bulk materials have been thoroughly studied, the chemical and structural modifications of 2D materials is still vastly an unexplored topic; it is only recently that it has attracted strong interest.[6,7] In particular, the chemical modification, doping, and other methods of varying material's physical properties can lead us to unexpected but exciting results and expand the sphere of applications of 2D materials.[8,9]

Gallium selenide has been gaining interest since the last few years, especially in applications such as photodetectors[10] and solar cells.[11] Also, there are large number of reports on the different characteristics of GaSe, from conductivity and nonlinear optical to photocatalytic properties.[12,13] Functionalization with plasmonic nanoparticles is a promising approach for the modification and control of 2D material properties.[14,15] Laser irradiation was employed to change the structure of GaSe. However, this approach leads to issues like accelerated GaSe decomposition or oxidation in ambient conditions.[16−18] Even low-powered irradiation (3−5 mW) and wavelengths close to the infrared (IR) spectrum have been reported to induce GaSe decomposition.[19]

Patterning by pulsed laser irradiation and fabrication of nanostructures with their characteristic dimensions below the wavelength of the laser was studied mainly on thin metal films.[20] For 2D materials, mostly femtosecond (FS) laser ablation and nanopatterning of graphene was studied.[21,22] In particular, fabrication of multilayer graphene nanoribbon arrays was demonstrated *via* laser-induced periodic surface structuring,[23,24] and connected to surface-plasmon effects.[23] Besides nanoscale patterning of graphene, laser-thinning $MoS_2$ was demonstrated with FS pulses, allowing for patterning,

**Received:** March 10, 2020
**Accepted:** April 13, 2020
**Published:** April 24, 2020




https://dx.doi.org/10.1021/acsomega.0c01079
*ACS Omega* 2020, 5, 10183−10190

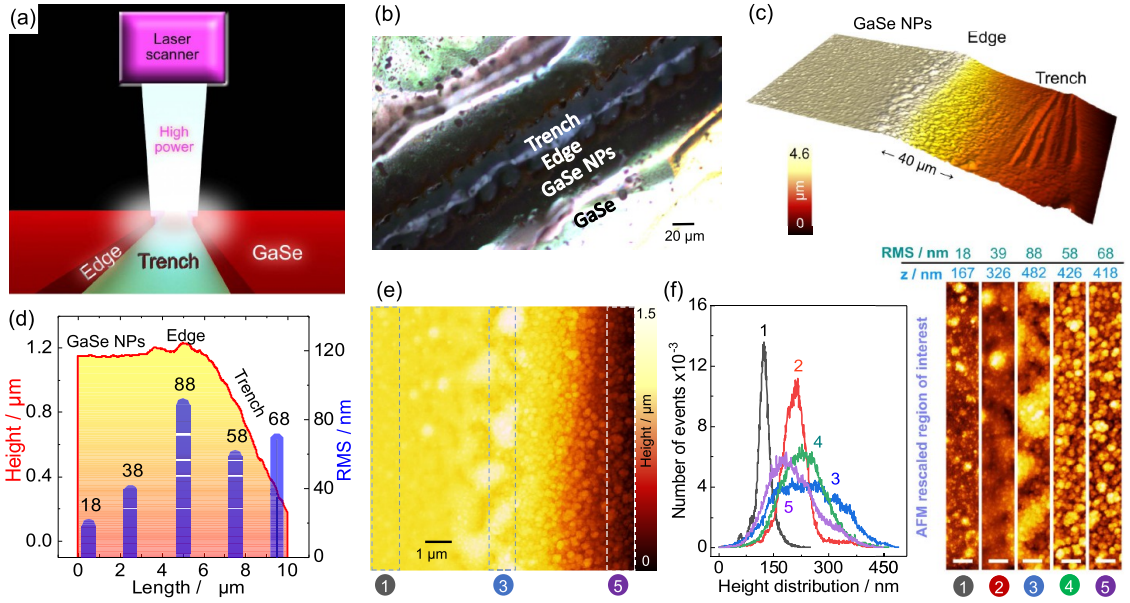


**Figure 1.** (a) Illustration of the high-power laser processing of GaSe using a computer-controlled laser scanner. (b) Optical microscopy image showing the regions of interest. (c) Three-dimensional (3D) AFM topography of the laser-irradiated GaSe surface. (d) Cross section of the middle part of (c), perpendicular to the trench direction, also shows the corresponding surface roughness. (e) AFM topography image of GaSe edge. (f) Height distributions (histograms) for nanoparticles shown in the Z-scale images and the roughness from different regions numbered from 1 to 5. These five images are rescaled regions from sections in (e). The scale bars are 1 $\mu$m.

controlling, and selecting the desired film thickness.[25,26] Besides FS laser ablation-based methods for nanoscale patterning of 2D materials, optothermoplasmonic nanolithography was also established for graphene and $MoS_2$,[27] however, this approach relies on gold nanoparticles as plasmonic support to reduce required laser power, and to bypass FS operation regime.

In contrast to those previous studies, our work aims at investigating the effects of GaSe irradiation in the air by a semiconductor laser with a wavelength near the UV spectrum (405 nm) and a laser excitation power in the range of 1 W. Assuming the ablation of the material under the laser's beam, we revealed that GaSe survived such conditions on the edges of the irradiated zone. To our surprise, we observed the formation of a large number of nanoparticles on the edges at the periphery of the laser-ablated region (herein called trench). Nanoparticle formation by laser irradiation was also previously reported for the case of laser-thinned $MoS_2$ films. The nanoparticles acted as nucleation sites, with size and distribution reported to depend on layer thickness and power density.[28] Similar phenomena of nanoparticle formation were observed upon laser ablation of metallic layers, especially in liquid environments.[29,30] Raman spectroscopy, atomic force microscopy (AFM), dielectric force microscopy (DFM), and scanning electron microscopy (SEM) results showed that the nanoparticles formed remain to a large extent GaSe. Their deviation from the original material in terms of structure, light scattering, and quantitative elementary content is discussed in this article. We did not find evidence of oxidation but only a minor presence of $Ga_2Se_3$. Finally, we studied the spatially controlled laser modification of GaSe for photocatalysis. Laser processing gave us a way to increase the GaSe photocatalytic activity in combination with Ag composite nanostructures selectively formed on the laser-irradiated regions.

## RESULTS AND DISCUSSION

Results obtained from AFM topography analyses showed that a large number of nanoparticles (herein called NPs) were formed in several micrometer wide regions next to the laser-ablated trench (see Figure 1).

The trench formed due to laser ablation is visible in the optical microscopy image in Figure 1b. We also noticed that the material on the edge of the laser-irradiated line had different morphology from the original flat and smooth two-dimensional GaSe. This observation was possible from the AFM result in Figure 1c. We found that the GaSe roughness and topography changed in the direction perpendicular to the laser-irradiated edge as evidenced in Figure 1d. A closer look at the region around the edge (AFM result in Figure 1e) shows the presence of NPs with different size distributions (Figure 1f). The results in Figure 1f were extracted from the AFM image in Figure 1e, by plotting histograms and rescaled sections numbered from 1 to 5. The appearance of NPs upon laser irradiation was also reported for the case of $MoS_2$ layers before laser power reached levels to induce layer thinning.[28,31] GaSe was studied by Raman spectroscopy in the near-infrared (NIR) and visible excitation wavelengths. Although for laser processing we used a power density higher than in our Raman experiments, the laser wavelength in the near-UV played a crucial role in the edge formation. For instance, our Raman spectroscopy results under green laser excitation showed decomposition of the pristine GaSe but not material removal or nanoparticle formation. That is why for the Raman spectroscopy analyses we had to limit laser excitation to the NIR spectral range (785 nm) for which decomposition was not noticeable. These observations confirm the significant role of laser energy that is leveraged by a high-power density induced ablation and nanoparticle formation at the edges. We did not observe these modifications for lower laser powers or lower photon energies using other lasers in our Raman experiments. One of the most significant observations is the persistence of


https://dx.doi.org/10.1021/acsomega.0c01079
ACS Omega 2020, 5, 10183−10190

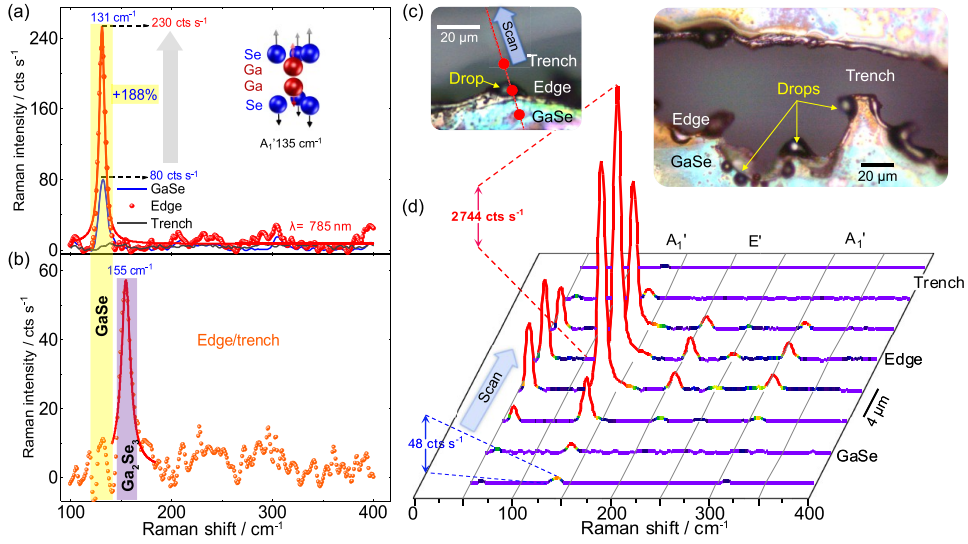


**Figure 2.** (a) Intensity of Raman peak on laser-treated area exceeds the Raman peak intensity from pristine GaSe by around a factor of 3. The symmetry of the main GaSe mode is also illustrated. (b) On the edge region, closer to the trench, a Raman peak at 155 $cm^{-1}$ appears that is representative of the $Ga_2Se_3$ phase. (c) Microscopy images showing the line with spots where Raman spectra were recorded in (d), recrystallized edges and drops. (d) Raman spectra from spots on the line in (c); scan along the GaSe/Edge/"drop"/Trench interface of a laser irradiated line showing an increase of $A_1'$ Raman mode intensity on the GaSe drops by almost 60 times when compared with the pristine GaSe surface.

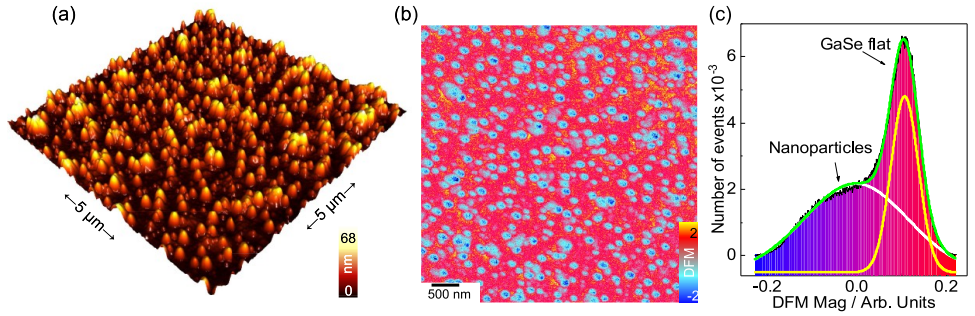


**Figure 3.** (a) Atomic force microscopy topography image of the GaSe region around the edge. This region is characterized by the presence of well-dispersed nanoparticles. (b) Dielectric force microscopy amplitude image showing the contrast between the flat GaSe and the nanoparticles. (c) Histogram of the DFM image showing the distribution into two components approximated by Gaussian fits.

the GaSe phase after such an aggressive high-power laser treatment. This is reflected by the spatially-resolved Raman spectroscopy results (Figure 2) that show a significant intensity increase of GaSe peaks at the edges formed by laser irradiation. Figure 2a demonstrates that the Raman peaks from edges are sharper (full width at half-maximum (FWHM) = 6 $cm^{-1}$) than those of the pristine GaSe flake (FWHM = 9 $cm^{-1}$). However, these FWHM changes are not that large for the spectra shown in Figure 2d acquired for another sample; but we still systematically observe a much higher GaSe intensity at the edges. We hypothesize that melting and recrystallization of GaSe along the laser-irradiated edge occur as a consequence of photothermal heating. Meanwhile, photothermal effects from laser irradiation were also used for thinning 2D materials like $MoS_2$.[28] Laser-thinning multilayered graphene enabled single-layers without chemical transformation under ambient conditions thanks to optical interference and localized heat-dissipation mediated by the $SiO_2$ substrate showing the impact of photothermal heating in 2D materials.[32] In Figure 2c, we see indications of this heating along the lines as evidenced by the presence of structures with a metallic luster, and in some instances, spherical particles that appear to be converted to drops from a liquid phase.[33] The likely scenario that explains the formation of spherical structures shown in Figure 2c is by considering this as a result of cooling down a liquid phase formed during laser irradiation. Hence, the higher crystallinity of laser-irradiated structures implies an increase in lattice order that should improve the electronic properties of GaSe. In addition, compared to Raman peaks from pristine GaSe, the peak intensity on modified zones increased.

We initially assumed that the increase in intensity observed in the Raman spectra was a consequence of the high-power irradiation that induced the redeposition of ablated material, increasing the amount of GaSe at the edges. This expectation is reasonable since the material ejected during laser ablation must have ended up somewhere, and at least a part of it should have deposited around the edges and also inside the trench. This was also noticed in a previous report on $MoS_2$.[31] Thus, we looked into the evidence for the material redeposition from Raman spectroscopy (and energy-dispersive X-ray spectroscopy (EDX) analyses discussed below), but we could not find conclusive results. Moreover, the AFM results show that there is an insignificant change in topography relative to the change in Raman intensity peaks. This observation rules out the hypothesis of a more significant amount of GaSe as an explanation for the increase in Raman signal at the edges. This


https://dx.doi.org/10.1021/acsomega.0c01079
ACS Omega 2020, 5, 10183−10190

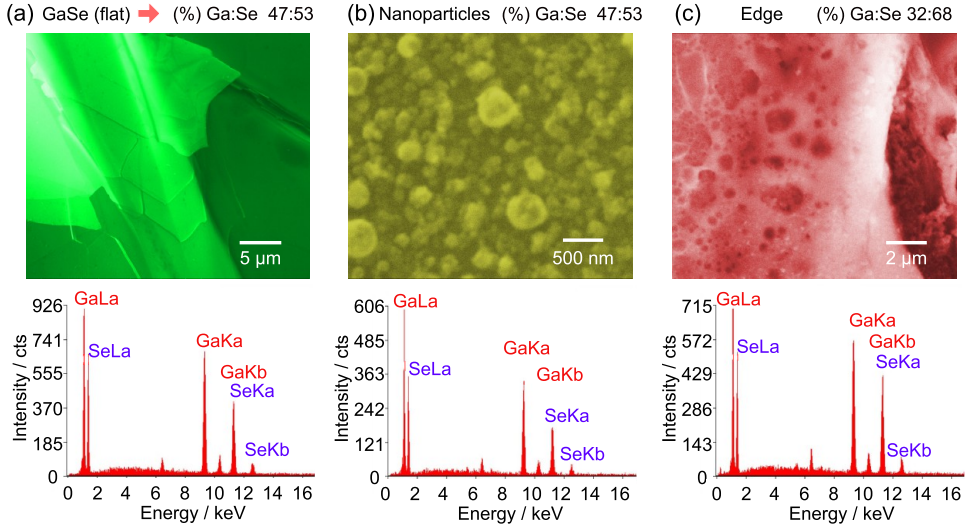


**Figure 4.** Scanning electron microscopy analysis of the laser-irradiated GaSe sample over representative regions of interest, pristine GaSe, close to the edge dominated by nanoparticles, and the edge made by the high-power laser. The elemental analysis by energy-dispersive X-ray spectroscopy shows that the Ga/Se ratio decreases at the edge with respect to the values over the pristine substrate and the region rich in nanoparticles.

result is contrary to the case of high-powered laser processing graphene oxide films, which also involved material ablation but with a vast topography increase at the edges.[34] Notice also that the spectra collection during the Raman line scan in Figure 2 did not cover only spherical structures that have a larger volume but also flatter regions. Thus, higher intensity might also occur due to changes in the physical or chemical properties of GaSe. Based on our observations discussed above, it is then reasonable to assume that material at the edges recrystallized and thus the energy band gap should have also changed. This assumption can be justified by considering that the physical origin of the electronic band gap stems from an effective crystal-field acting on the GaSe electrons. If the lattice order changes, then the crystal field also changes, affecting the energy band gap. Thus, the band gap change can also bring the modified GaSe system closer to preresonance conditions with the laser excitation (785 nm) used in our Raman experiments. Such an amelioration of the preresonance conditions resulting from the change in the band gap accounts for the observed enhancement in Raman intensity.

Changing the GaSe morphology by particle formation implies that charge-carrier mobility changes as well. This hypothesis was supported by dielectric force microscopy (DFM) results presented in Figure 3. There are few obstacles preventing electrons from moving in two-dimensional GaSe, such as charge-carrier scattering with phonons, defects, and other charge carriers. In the process of scanning the sample by DFM, at each point, the capacitance of the probe surface system changes due to differences in the content and mobility of charge carriers. Hence, the formed particles in the laser-treated area, and particularly their surface, represent a large number of scattering centers for charge carriers. With about 800 nanoparticles per 1600 $\mu m^2$, as estimated from AFM results, it makes sense to expect that the mobility of charge carriers should decrease.

The DFM results show lower mobility of nanoparticles reflected by a decrease in image contrast[35] (see Figure 3). It is worth noticing that the nanoparticle formation after high-power laser processing could be a general observation in 2D semiconductors, like that reported for the laser thinning of the $MoS_2$ layers.[28] Figure 2b shows a new peak observed during the Raman line scan experiment that belongs to $Ga_2Se_3$.[36] Considering the phase diagram of gallium−selenium,[37] we expect that in some cases, if the laser can heat GaSe to a certain temperature (about 930 °C), the GaSe becomes $Ga_2Se_3$. The phase diagram explains our EDX results where we observed 70 wt % of selenium and 30 wt % of gallium for some locations at the edge of the laser-irradiated region.

Scanning electron microscopy (SEM) was used to investigate the sample at locations with pristine GaSe and regions close to the laser-ablated trench, including parts rich in GaSe nanoparticles. SEM results (Figure 4) are in agreement with the data obtained by AFM-based techniques (Figures 1 and 3). This refers to the spherical shape of the nanoparticles, their sizes, and their density with respect to the distance from the trench.

The SEM images and EDX results shown in Figure 4 demonstrate a noticeable decrease in the Ga/Se ratio at the laser-irradiated edge. GaSe has an ideal composition with 50% content of gallium and 50% content of selenium. After laser illumination around the edge, the Se content increased with respect to Ga, suggesting the formation of the $Ga_2Se_3$ phase discussed above.

Compared with laser-processed $MoS_2$, especially with laser thinning that involves high-power laser irradiation, previous work showed that Mo oxide formation did not occur for laser intensities below 1 mW.[31] More recently, the same group showed that nanoparticles without oxidation occurred as a preliminary stage to laser thinning under moderate power densities.[28] Furthermore, although there was a high power density at the laser spot, the power density is much lower at its periphery such that NP oxidation was avoided. However, the exact mechanism of nanoparticle formation and ruling out oxidation still elude us. This open question could be addressed using more sensitive analytical techniques such as micro-XPS with sufficient spatial resolution. The nature of nanoparticles obtained by laser processing will be investigated further in the follow-up work. For example, it would be interesting to capture the material ejected during ablation by placing a microscope glass directly on top of GaSe. By analyzing the deposits on the


https://dx.doi.org/10.1021/acsomega.0c01079
ACS Omega 2020, 5, 10183−10190

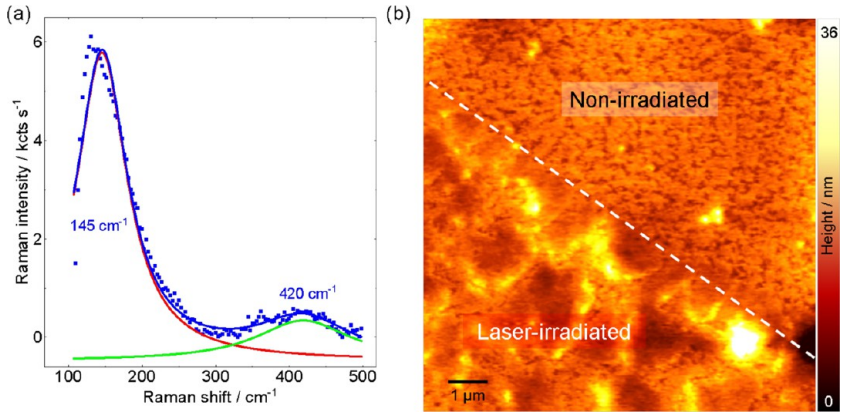


**Figure 5.** (a) Raman spectra obtained after deposition of $AgNO_3$ solution on the GaSe surface. Solid lines in (a) represent Lorentzian fits; peak positions are also provided. (b) Atomic force microscopy of the laser-irradiated region interface on GaSe after contact with $AgNO_3$.

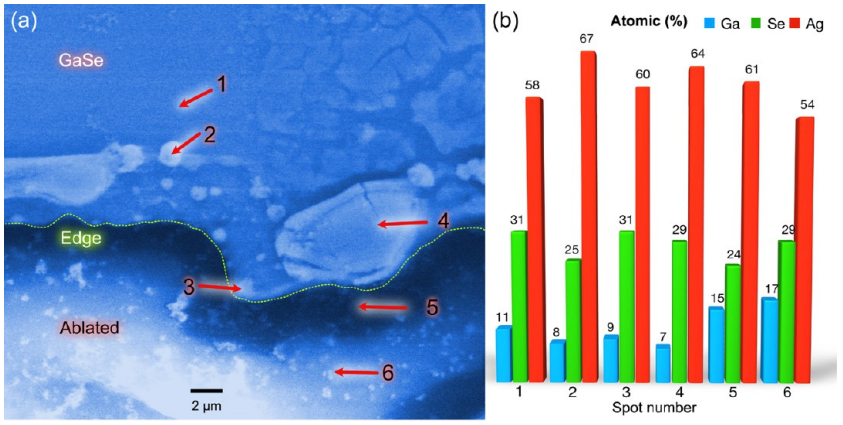


**Figure 6.** (a) SEM images of the GaSe surface after dropping the solution of $AgNO_3$. The dashed line is a guide highlighting the edge. (b) EDX histogram of the distribution of elements on the sample.

glass after laser processing, we could determine the nature of nanoparticles captured and compared with the nanoparticles deposited at the edges.

**Selective Nanostructuring and Photocatalytic Activity of Ag-Functionalized GaSe Laser-Ablated Edges.** To highlight the effects of high-powered laser processing on GaSe edges, the photocatalytic properties were investigated. We are motivated by photocatalysis since the edges that are left after ablation have a higher photoinduced damage threshold than the pristine GaSe.[38] This localized modification, in addition to nonstoichiometric GaSe at the edge due to surface defects, is expected to increase the photocatalytic activity of this material as reported for the case of $MoS_2$.[39] For the photocatalysis experiment, we chose 4-nitrobenzenethiol (4NBT) solution as an indicator of catalytic activity. 4NBT undergoes catalytic reaction in the presence of chemical reductants or plasmonic nanoparticles.[40,41]

GaSe shows no transformation of 4NBT to 4-aminobenzenthiol (4ABT) or dimerization to 4,4′-dimercaptoazobenzene (DMBA), probably due to the p-type semiconductor nature of GaSe. We expect that the laser irradiation process gives rise to surface-active sites that promote the growth of photocatalytically active nanostructures. To test this hypothesis, the GaSe samples were immersed in 5 mL of $AgNO_3$ 1% (4 mL of $AgNO_3$ and 396 mL of distilled water). Before investigating the photocatalytic activity, the material formed after this $AgNO_3$ functionalization step was investigated by Raman spectroscopy, atomic force microscopy, SEM, and elementary analysis with EDX. The Raman spectrum in Figure 5a shows that $AgNO_3$ reacts with GaSe to display a single broad peak around 145 cm$^{-1}$, attributed to $Ag_2Se$.[42] This result suggests the formation of a composite between Ag, Se, and Ga. The broader signal around 420 cm$^{-1}$ originates from other composites. The effect of laser irradiation on the formation of silver composite nanostructures is further evidenced in the AFM topography image (see Figure 5b). While $AgNO_3$ readily changes the surface topography of GaSe, this modification is largely enhanced by pretreatment with laser irradiation. These changes were also investigated with EDX elemental analysis. The SEM imaging in Figure 6a is used to locate the regions of interest that allowed EDX analyses, and the comparison is given in Figure 6b.

Notice that at this scale and image contrast, SEM does not show particles as opposed to the AFM imaging results discussed above. From the EDX results presented in Figure 6b, it is evident that the content of Ag increases closer to the edge, while the Se content reduces. Also, as Raman results suggest, after laser irradiation and reaction with $AgNO_3$, GaSe changed to a nanostructured composite of Ga, Se, and Ag. The elemental evaluation shows that these changes are not equal but Ag and Se dominate over Ga content. Finally, we investigate the photocatalytic properties of these nanostructures. For this, a solution of 4NBT was deposited on the sample's surface and left for 15 h. After this period, the sample


https://dx.doi.org/10.1021/acsomega.0c01079
ACS Omega 2020, 5, 10183−10190

was thoroughly rinsed with distilled water. The 4NBT molecular changes due to photocatalytic reactions were induced and monitored *in situ* under green laser excitation ($\lambda$ = 532 nm) by Raman spectroscopy.

Raman spectra recorded far from the edge show that 4NBT did not react with the flat GaSe surface as evidenced in Figure 7. The sharp $NO_2$ peak at 1336 $cm^{-1}$ from the original 4NBT

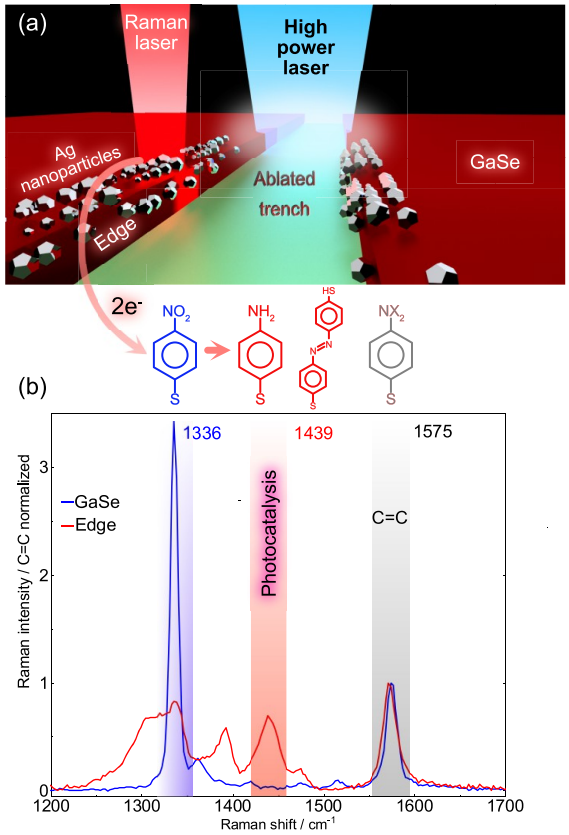


**Figure 7.** (a) Illustration of the Ag nanostructures around the laser-irradiated GaSe edge. (b) Raman spectra of $Ag_2Se$ with Ag nanoparticles and 4NBT as a molecular probe for photocatalytic activity.

molecule reflects the lack of photocatalytic activity in that region. In contrast, when moving closer to the edge, the intensity of the $NO_2$ peak decreases. At the same time, a peak from $\nu_{CC} + \delta_{CH}$ ring vibration (related to 4ABT and 4,4′-dimethylaminobenzaldehyde (DMAB)) appears at 1439 $cm^{-1}$.[41] This result implies that the $Ag_2Se$ nanostructures catalyzed the transformation of 4NBT molecules to 4-aminothiophenol and DMAB at the laser-irradiated interface. This reaction leads to the conversion of the nitro $NO_2$ group to the amino $NH_2$ group and the dimerization observed in the Raman spectra. This signature is a measure of the photocatalytic activity[43] that is spatially confined to the edge of the high-power laser-illuminated regions.

## CONCLUSIONS

We elucidated the effects of high-power laser processing of two-dimensional GaSe single crystals. Photothermal effects from laser irradiation resulted in material ablation and modification of GaSe at the periphery of the laser spot. The photothermal heating induced melting and recrystallization of GaSe around the edges of the trench formed by the laser. This recrystallization gave way to the formation of GaSe particles in addition to other phases identified by Raman spectroscopy and EDX. We found that the properties of these particles differ from those of pristine 2D GaSe. We attribute an enhanced Raman signal intensity to the band gap modification of GaSe. This band gap change increases the preresonance conditions, making GaSe electronic transitions more efficient with the laser excitation used. Deviation from stoichiometric GaSe was evidenced by elemental analysis using EDX, which shows a higher selenium content around the laser spot edge. This result, in addition to the observation of a Raman active mode at 155 $cm^{-1}$, indicates the formation of $Ga_2Se_3$ by laser irradiation. The higher chemical activity of laser-irradiated GaSe was verified by the selective growth of Ag composites as deduced by direct observation with atomic force microscopy. The spatially selective activity of the laser-irradiated regions allowed us to obtain Ag and $Ag_2Se$ nanostructures by reaction with a solution of $AgNO_3$. These nanostructures showed high photocatalytic activity reflected by the chemical transformation of 4NBT to 4ABT and 4DMBA. Thus, this work demonstrated the simultaneous patterning and added functionality to 2D GaSe single crystals by high-power laser irradiation with an impact on photocatalysis, optoelectronics, and flexible device applications.

## EXPERIMENTAL SECTION

A centimeter-sized GaSe single crystal grown by the Bridgman method was used as a source of multilayer flakes used in this work.[44] The sample was prepared by taking a micrometer thick layer from the GaSe single crystal by acrylic-based adhesive tape and fixing it on a glass with a double-sided adhesive tape. On the one hand, the chosen sample preparation method is straightforward and inexpensive. On the other hand, keeping the flakes fixed to the surface of the tape allows for multiple liquid immersions without the risk of sample delamination, which was particularly crucial for the photocatalytic experiments described in this paper. Delamination of flakes in liquids is an issue if commonly used supports as $Si/SiO_2$ substrates are employed. Also, the absence of unwanted influences from the adhesive tape in the spectra, AFM, and SEM EDX results prove the versatility of the preparation method. Violet (CW) laser with a wavelength of 405 nm, 1 W power, and 20 $\mu$m spot width was used in this study. One line was traced with a computer-controlled laser system by scanning twice with the laser spot on the same surface, and with exposition time of 100 ms/point in ambient conditions. Absence of $Ga_2O_3$ peaks in the Raman results means that GaSe was not oxidized.[45]

Raman spectroscopy analysis was performed with a Thermo Fisher Scientific DXR2 Raman microscope on different regions of interest, including the laser-irradiated line, its edge, and pristine GaSe. For Raman spectroscopy, laser excitation with 785 nm, power from 4 to 6 mW, and ×50 magnification were used. This near-IR laser excitation enabled us to observe the GaSe surface without decomposing, modifying, or inducing additional structural changes. The GaSe surface morphologies within the same regions of interest were obtained by an intermittent contact mode (tapping mode) operated by the NTEGRA NT-MDT AFM system. SEM and energy-dispersive X-ray spectroscopy (EDX) experiments were carried out with a QUANTA 200 3D on three areas of the surface nonaffected zone, edges of the laser line, and inside the trench, with ×10 000 and ×80 000 magnifications and HV of 30 kV.


https://dx.doi.org/10.1021/acsomega.0c01079
ACS Omega 2020, 5, 10183−10190

To explore the photocatalytic properties, a solution of 5 mL of $AgNO_3$ 1% (4 mL of $AgNO_3$ and 396 mL of distilled water) was drop-coated on the laser-irradiated surface and left overnight. Then, the sample was rinsed thoroughly with distilled water. Afterward, a 4-nitrobenzenethiol (4NBT) aqueous solution was dropped on the sample and left for 15 h, followed by another cleaning step. To investigate the photocatalytic activity of the Ag nanostructures formed on the laser-irradiated GaSe surface, Renishaw inVia Basis Raman spectrometer with an excitation wavelength of 532 nm, 0.5 mW power, and ×50 magnification was used.

## AUTHOR INFORMATION


### Corresponding Author

**Raul D. Rodriguez** − *Tomsk Polytechnic University, 634050 Tomsk, Russia;* orcid.org/0000-0003-4016-1469; Phone: +7-923-432-23-27; Email: raul@tpu.ru

### Authors

**Dmitry Cheshev** − *Tomsk Polytechnic University, 634050 Tomsk, Russia*

**Aleksandar Matković** − *Institute of Physics, Montanuniversität Leoben, 8700 Leoben, Austria*

**Alexey Ruban** − *Tomsk Polytechnic University, 634050 Tomsk, Russia*

**Jin-Ju Chen** − *School of Materials and Engineering, University of Electronic Science and Technology of China, 610054 Chengdu, China*

**Evgeniya Sheremet** − *Tomsk Polytechnic University, 634050 Tomsk, Russia;* orcid.org/0000-0003-3937-8628

Complete contact information is available at: https://pubs.acs.org/10.1021/acsomega.0c01079


### Notes

The authors declare no competing financial interest.

## ACKNOWLEDGMENTS

We thank Santos Adán López Rivera, who synthesized the most impressive single crystals. We thank Chaschin Vladimir and Khokhlov Maxim for helping to start this work. This work was funded by RFBR and FWF research project No. 19-52-14006. A.M. acknowledges the support by the Austrian Science Fund (FWF Der Wissenschaftsfonds) through project I4323-N36. This research is supported by the Tomsk Polytechnic University within the framework of the Tomsk Polytechnic University Competitiveness Enhancement Program, 5-100, and by the Sichuan Science and Technology Program (Grant 2018HH0152).

## REFERENCES


(1) Ben Aziza, Z.; Henck, H.; Pierucci, D.; Silly, M. G.; Lhuillier, E.; Patriarche, G.; Sirotti, F.; Eddrief, M.; Ouerghi, A. Van Der Waals Epitaxy of GaSe/Graphene Heterostructure: Electronic and Interfacial Properties. *ACS Nano* **2016**, *10*, 9679−9686.

(2) Ferrari, A. C.; Bonaccorso, F.; Fal'ko, V.; Novoselov, K. S.; Roche, S.; Bøggild, P.; Borini, S.; Koppens, F. H. L.; Palermo, V.; Pugno, N.; et al. Science and Technology Roadmap for Graphene, Related Two-Dimensional Crystals, and Hybrid Systems. *Nanoscale* **2015**, *7*, 4598−4810.

(3) Thu, N. T. A.; Cuong, N. D.; Nguyen, L. C.; Khieu, D. Q.; Nam, P. C.; Toan, N. V.; Hung, C. M.; Hieu, N. V. Fe2O3 Nanoporous Network Fabricated from Fe3O4/reduced Graphene Oxide for High-Performance Ethanol Gas Sensor. *Sens. Actuators, B* **2018**, *255*, 3275−3283.

(4) Cai, X.; Luo, Y.; Liu, B.; Cheng, H.-M. Preparation of 2D Material Dispersions and Their Applications. *Chem. Soc. Rev.* **2018**, *47*, 6224−6266.

(5) Xie, C.; Mak, C.; Tao, X.; Yan, F. Photodetectors Based on Two-Dimensional Layered Materials Beyond Graphene. *Adv. Funct. Mater.* **2017**, *27*, No. 1603886.

(6) Guo, Y.; Xu, K.; Wu, C.; Zhao, J.; Xie, Y. Surface Chemical-Modification for Engineering the Intrinsic Physical Properties of Inorganic Two-Dimensional Nanomaterials. *Chem. Soc. Rev.* **2015**, *44*, 637−646.

(7) Rodriguez, R. D.; Khalelov, A.; Postnikov, P. S.; Lipovka, A.; Dorozhko, E.; Amin, I.; Murastov, G. V.; Chen, J.-J.; Sheng, W.; Trusova, M. E.; et al. Beyond Graphene Oxide: Laser Engineering Functionalized Graphene for Flexible Electronics. *Mater. Horiz.* **2020**, *7*, 1030−1041.

(8) Genovese, L.; Cocchiara, C.; Patella, B.; Sunseri, C.; Inguanta, R. Synthesis of Silver Gallium Selenide (AgGaSe2) Nanotubes and Nanowires by Template-Based Electrodeposition. *J. Nanosci. Nanotechnol.* **2020**, *20*, 999−1007.

(9) Sheng, W.; Amin, I.; Neumann, C.; Dong, R.; Zhang, T.; Wegener, E.; Chen, W.-L.; Förster, P.; Tran, H. Q.; Löffler, M.; et al. Polymer Brushes on Hexagonal Boron Nitride. *Small* **2019**, *15*, No. 1805228.

(10) Sorifi, S.; Moun, M.; Kaushik, S.; Singh, R. High Temperature Performance of GaSe Nanosheet Based Broadband Photodetector. *ACS Appl. Electron. Mater.* **2020**, *2*, 670−676.

(11) Ramanujam, J.; Singh, U. P. Copper Indium Gallium Selenide Based Solar Cells − a Review. *Energy Environ. Sci.* **2017**, *10*, 1306−1319.

(12) Mo, X.; Chan, K. C.; Tse, E. C. M. A Scalable Laser-Assisted Method to Produce Active and Robust Graphene-Supported Nanoparticle Electrocatalysts. *Chem. Mater.* **2019**, *31*, 8230−8238.

(13) Zhuang, H. L.; Hennig, R. G. Single-Layer Group-III Monochalcogenide Photocatalysts for Water Splitting. *Chem. Mater.* **2013**, *25*, 3232−3238.

(14) Li, X.; Zhu, J.; Wei, B. Hybrid Nanostructures of Metal/two-Dimensional Nanomaterials for Plasmon-Enhanced Applications. *Chem. Soc. Rev.* **2016**, *45*, 3145−3187.

(15) Sheng, W.; Li, W.; Tan, D.; Zhang, P.; Zhang, E.; Sheremet, E.; Schmidt, B. V. K. J.; Feng, X.; Rodriguez, R. D.; Jordan, R.; Amin, I.; et al. Polymer Brushes on Graphitic Carbon Nitride for Patterning and as a SERS Active Sensing Layer via Incorporated Nanoparticles. *ACS Appl. Mater. Interfaces* **2020**, *12*, 9797−9805.

(16) Shi, L.; Li, Q.; Ouyang, Y.; Wang, J. Effect of Illumination and Se Vacancies on Fast Oxidation of Ultrathin Gallium Selenide. *Nanoscale* **2018**, *10*, 12180−12186.

(17) Bereznaya, S. A.; Korotchenko, Z. V.; Novikov, V. A.; Redkin, R. A.; Sarkisov, S. Y.; Atuchin, V. V. Formation of Native Oxide Crystallites on GaSe(0 0 1) Surface. *Infrared Phys. Technol.* **2016**, *76*, 126−130.

(18) Rahaman, M.; Rodriguez, R. D.; Monecke, M.; Lopez-Rivera, S. A.; Zahn, D. R. T. GaSe Oxidation in Air: From Bulk to Monolayers. *Semicond. Sci. Technol.* **2017**, *32*, No. 105004.

(19) Novikov, V. A.; Sarkisov, S. Y. Formation of Intrinsic Oxide Nanocrystals on the Surface of GaSe under Laser Irradiation. *J. Surf. Invest.: X-Ray, Synchrotron Neutron Tech.* **2016**, *10*, 738−741.

(20) Ruffino, F.; Grimaldi, M. G. Nanostructuration of Thin Metal Films by Pulsed Laser Irradiations: A Review. *Nanomaterials* **2019**, *9*, No. 1133.

(21) Sahin, R.; Simsek, E.; Akturk, S. Nanoscale Patterning of Graphene through Femtosecond Laser Ablation. *Appl. Phys. Lett.* **2014**, *104*, No. 053118.

(22) Gil-Villalba, A.; Meyer, R.; Giust, R.; Rapp, L.; Billet, C.; Courvoisier, F. Single Shot Femtosecond Laser Nano-Ablation of CVD Monolayer Graphene. *Sci. Rep.* **2018**, *8*, No. 14601.

(23) Beltaos, A.; Kovačević, A. G.; Matković, A.; Ralević, U.; Savić-Šević, S.; Jovanović, D.; Jelenković, B. M.; Gajić, R. Femtosecond Laser Induced Periodic Surface Structures on Multi-Layer Graphene. *J. Appl. Phys.* **2014**, *116*, No. 204306.

(24) Kovalska, E.; Pavlov, I.; Deminskyi, P.; Baldycheva, A.; Ilday, F. Ö.; Kocabas, C. NLL-Assisted Multilayer Graphene Patterning. *ACS Omega* **2018**, *3*, 1546−1554.
(25) Castellanos-Gomez, A.; Barkelid, M.; Goossens, A. M.; Calado, V. E.; van der Zant, H. S. J.; Steele, G. A. Laser-Thinning of MoS2: On Demand Generation of a Single-Layer Semiconductor. *Nano Lett.* **2012**, *12*, 3187−3192.
(26) Hu, L.; Shan, X.; Wu, Y.; Zhao, J.; Lu, X. Laser Thinning and Patterning of MoS2 with Layer-by-Layer Precision. *Sci. Rep.* **2017**, *7*, No. 15538.
(27) Lin, L.; Li, J.; Li, W.; Yogeesh, M. N.; Shi, J.; Peng, X.; Liu, Y.; Rajeeva, B. B.; Becker, M. F.; Liu, Y.; et al. Optothermoplasmonic Patterning: Optothermoplasmonic Nanolithography for On-Demand Patterning of 2D Materials (Adv. Funct. Mater. 41/2018). *Adv. Funct. Mater.* **2018**, *28*, No. 1870299.
(28) Tran-Khac, B.-C.; White, R. M.; DelRio, F. W.; Chung, K.-H. Layer-by-Layer Thinning of MoS2 via Laser Irradiation. *Nanotechnology.* **2019**, *30*, No. 275302.
(29) Dolgaev, S. I.; Simakin, A. V.; Voronov, V. V.; Shafeev, G. A.; Bozon-Verduraz, S. F. Nanoparticles Produced by Laser Ablation of Solids in Liquid Environment. *Appl. Surf. Sci.* **2002**, *186*, 546−551.
(30) Itina, T. E. On Nanoparticle Formation by Laser Ablation in Liquids. *J. Phys. Chem. C* **2011**, *115*, 5044−5048.
(31) Alrasheed, A.; Gorham, J. M.; Tran Khac, B. C.; Alsaffar, F.; DelRio, F. W.; Chung, K.-H.; Amer, M. R. Surface Properties of Laser-Treated Molybdenum Disulfide Nanosheets for Optoelectronic Applications. *ACS Appl. Mater. Interfaces* **2018**, *10*, 18104−18112.
(32) Han, G. H.; Chae, S. J.; Kim, E. S.; Güneş, F.; Lee, I. H.; Lee, S. W.; Lee, S. Y.; Lim, S. C.; Jeong, H. K.; Jeong, M. S.; et al. Laser Thinning for Monolayer Graphene Formation: Heat Sink and Interference Effect. *ACS Nano* **2011**, *5*, 263−268.
(33) Zavrazhnov, A. Y.; Turchen, D. N.; Naumov, A. V.; Zlomanov, V. P. Chemical Transport Reactions as a New Variant of the Phase Composition Control. *J. Phase Equilib.* **2003**, *24*, 330−339.
(34) Rodriguez, R. D.; Murastov, G. V.; Lipovka, A.; Fatkullin, M. I.; Nozdrina, O.; Pavlov, S. K.; Postnikov, P. S.; Chehimi, M. M.; Chen, J.-J.; Sheremet, E. High-Power Laser-Patterning Graphene Oxide: A New Approach to Making Arbitrarily-Shaped Self-Aligned Electrodes. *Carbon* **2019**, *151*, 148−155.
(35) Zhang, J.; Lu, W.; Li, Y. S.; Cai, J.; Chen, L. Dielectric Force Microscopy: Imaging Charge Carriers in Nanomaterials without Electrical Contacts. *Acc. Chem. Res.* **2015**, *48*, 1788−1796.
(36) Bletskan, D. I.; Kabatsii, V. N.; Kranjčec, M. Photoelectric Properties of Ordered-Vacancy Ga2Se3 Single Crystals. *Inorg. Mater.* **2010**, *46*, 1290−1295.
(37) Yamada, A.; Kojima, N.; Takahashi, K.; Okamoto, T.; Konagai, M. Raman Study of Epitaxial Ga2Se3Films Grown by Molecular Beam Epitaxy. *Jpn. J. Appl. Phys.* **1992**, *31*, L186−L188.
(38) Golubev, A. A.; Khlebtsov, B. N.; Rodriguez, R. D.; Chen, Y.; Zahn, D. R. T. Plasmonic Heating Plays a Dominant Role in the Plasmon-Induced Photocatalytic Reduction of 4-Nitrobenzenethiol. *J. Phys. Chem. C* **2018**, *122*, 5657−5663.
(39) Xie, J.; Zhang, H.; Li, S.; Wang, R.; Sun, X.; Zhou, M.; Zhou, J.; Lou, X. W. D.; Xie, Y. Defect-Rich MoS2 Ultrathin Nanosheets with Additional Active Edge Sites for Enhanced Electrocatalytic Hydrogen Evolution. *Adv. Mater.* **2013**, *25*, 5807−5813.
(40) Huang, Y.-F.; Zhu, H.-P.; Liu, G.-K.; Wu, D.-Y.; Ren, B.; Tian, Z.-Q. When the Signal Is Not from the Original Molecule To Be Detected: Chemical Transformation Ofpara-Aminothiophenol on Ag during the SERS Measurement. *J. Am. Chem. Soc.* **2010**, *132*, 9244−9246.
(41) Kong, X.; Zhu, H.; Chen, C.; Huang, G.; Chen, Q. Insights into the Reduction of 4-Nitrophenol to 4-Aminophenol on Catalysts. *Chem. Phys. Lett.* **2017**, *684*, 148−152.
(42) Ge, J.-P.; Xu, S.; Liu, L.-P.; Li, Y.-D. A Positive-Microemulsion Method for Preparing Nearly Uniform Ag2Se Nanoparticles at Low Temperature. *Chemistry* **2006**, *12*, 3672−3677.
(43) Hasell, T.; Lagonigro, L.; Peacock, A. C.; Yoda, S.; Brown, P. D.; Sazio, P. J. A.; Howdle, S. M. Silver Nanoparticle Impregnated Polycarbonate Substrates for Surface Enhanced Raman Spectroscopy. *Adv. Funct. Mater.* **2008**, *18*, 1265−1271.
(44) Ni, Y.; Wu, H.; Huang, C.; Mao, M.; Wang, Z.; Cheng, X. Growth and Quality of Gallium Selenide (GaSe) Crystals. *J. Cryst. Growth* **2013**, *381*, 10−14.
(45) Zhang, J.; Jiang, F. Catalytic Growth of Ga2O3 Nanowires by Physical Evaporation and Their Photoluminescence Properties. *Chem. Phys.* **2003**, *289*, 243−249.


https://dx.doi.org/10.1021/acsomega.0c01079
*ACS Omega* 2020, 5, 10183−10190